Characterization of a New Efflorescence Salt on Calcareous Historic Objects stored in Wood Cabinets: $Ca_2(CH_3COO)(HCOO)(NO_3)_2 \cdot 4H_2O$

SEBASTIAN BETTE[A]*, GERHARD EGGERT[B], ANDREA FISCHER[B], JÖRG STELZNER[B], ROBERT E. DINNEBIER[A]

[a]Max-Planck-Institute for Solid State Research, Heisenbergstr. 1 70569 Stuttgart, Germany
E-Mail: S.Bette@fkf.mpg.de
[b]State Academy of Art and Design, Am Weißenhof 1, 70191 Stuttgart, Germany

Abstract

White efflorescence crystals grown on the surfaces of a bronze bowl, classical ceramic and ancient wine jugs were investigated. X-ray powder diffraction (XRPD) revealed that in each case an identical, hitherto unknown phase was formed. The crystal structure was solved from high resolution XRPD measurements and revealed a phase composition of $Ca_2(CH_3COO)(HCOO)(NO_3)_2 \cdot 4H_2O$, which is in accordance with the complementary analysis. The overall structural motif of $Ca_2(CH_3COO)(HCOO)(NO_3)_2 \cdot 4H_2O$, one dimensional calcium carboxylate zig zag chains in which acetate and formate ions are arranged in an alternating fashion, is closely related to other naturally occurring or artificial efflorescence salts like thecotrichite or calclacite.

Keywords: A. ceramics; B. X-ray powder diffraction; B. Raman spectroscopy; B. SEM; C. atmospheric corrosion; C acid corrosion

1. Introduction

Wood, especially oak, emits some formic and acetic acid the latter being ester bound in the wood polyoses ("hemicellulose"). In situations with limited air exchange as in cupboards or drawers, typically hundred to thousand ppb can be measured[1]. These pollutants may cause damage on sensitive artefacts stored for long time in them under such conditions. Acetate containing efflorescence on calcareous natural history specimen like shells ("Byne's disease") has already been reported end of the 19th century[2]. Calcium acetates, often exhibiting needle like shape, have also been detected occurring on ceramics. During soil logging, calcareous accretions may be deposited on ceramics. Whether calcium from the ceramic body itself can also be mobilized to form calcium acetates has not been thoroughly studied yet, at least some clays are rich in calcium and are used for yellow wares. On fossils and limestone stored in wooden museum cases, on pottery sherds[3] including classical ceramics from the Agora of Athens stored in oak drawers and cabinets[4], calcium acetate hemihydrate and calclacite ($Ca(CH_3COO)Cl{\cdot}5H_2O$) have been detected in efflorescence. The pattern of calclacite could be indexed with a monoclinic unit cell[3,5] and it's crystal structure was already solved in 1972[6]. The chloride was attributed to the former practice of cleaning the ceramic sherds from the calcareous accretions with hydrochloric acid and directly drying them without prior soaking with water. This must have left considerable amounts of calcium chloride in the porous ceramic body. Especially on tiles which can take up migrating soluble salts from walls thecotrichite, a compound also containing nitrate, was detected[7]. Its exact formula, $Ca_3(CH_3COO)_3Cl(NO_3)_2{\cdot}6H_2O$, and its crystal structure have recently been determined[8].

The chemistry and the crystallography of calcium acetate and formate salts are rather complex, as for anhydrous calcium formate four distinct polymorphs[9,10] and for anhydrous calcium acetate three distinct polymorphs[11] are known. Crystal structures of calcium acetate formates are unknown so far although they are reported from molluscs in oak cabinets[12]. A pronounced polymorphism was also observed for calcium acetate monohydrate. Different polymorphs can be obtained when the phase is crystallized in pure water[13], water ethanol mixtures[14] or in presence of organic admixtures[15]. Calcium acetate hemihydrate ($Ca(CH_3COO)_2{\cdot}0.5H_2O$) was identified as an efflorescence product as well[4] but it's crystal structure remains still unknown. This phase occurs as an intermediary product of the thermal decomposition of calcium acetate monohydrate[16]. In aqueous solution the monohydrate phase was found to be thermodynamically stable[17]. The occurrence of the hemihydrate phase as an efflorescence product can be understood from the relative humidity (rH)-temperature diagram for the calcium acetate phases[4]. At room temperature, the monohydrate transforms to the hemihydrate below 71% rH. The systems $Ca(CH_3COO)_2$-$CaCl_2$-H_2O and $Ca(CH_3COO)_2$-$Ca(NO_3)_2$-H_2O have been studied systematically in order to find a thermodynamic explanation for the formation of calclacite and thecotrichte[4,18]. At 25 °C calclacite was found to crystallize in (3-7) *m* $CaCl_2$ solutions with a calcium acetate concentration from 0.1 to 1.4 mol/ kg (H_2O). The investigation on the system $Ca(CH_3COO)_2$-$Ca(NO_3)_2$-H_2O resulted in the discovery and characterization of an additional, artificial efflorescence salt $Ca_2(CH_3COO)_3NO_3{\cdot}2H_2O$[19]. Despite their occurrence as efflorescence, the system calcium acetate-calcium formate lacks a systematic study.

As needle like, white efflorescence crystals can be visually easily mistaken for thecotrichite or calclacite, calcareous efflorescence were sampled in natural history and historic collections in the framework of the

RaCoPhInO ("**Ra**re **Co**rrosion **Ph**enomena of **In**organic **O**bjects") research in the Objects' Conservation program of the State Academy of Art and Design Stuttgart. In four cases the same unknown compound was detected by X-ray powder diffraction (XRPD). One of the samples was evaluated to contain the new efflorescence phase without any impurities and used for a detailed characterization. As no suitable crystal for single crystal diffraction was found, the crystal structure was solved from XRPD measurements.

2. Materials and Methods

2.1.Sample Collection

Four samples of white efflorescence crystal were collected from four different objects, which were stored in three different museums (Table 1) under different conditions (relative humidity, temperature, furniture, etc.). The first object investigated here is an Anatolian copper alloy bowl from the Rautenstrauch-Joest-Museum Cologne bought from an antiquities trader in the bazaar of Istanbul and a few hundred years old. On the surface of the bowl turquoise coloured sections attributed to corrosion of the bronze material can be found besides white efflorescence crystals having a needle like shape (Fig. 1). Needle like white efflorescence crystals were found on the inner and outer side of an Attic black figured amphora depicting a bridal and a warrior procession of the Antikensammlung Munich (Fig. 2), excavated near Vulci (Italy) and bought in 1831 on behalf of Ludwig I. of Bavaria from the Candelori Collection. Two black figured Attic wine jugs[20], ca. 500 BCE (Fig. 3) from the National Museum of Antiquities Leiden also exhibit white efflorescence crystals.

Fig. 1. Anatolian copper alloy bowl (Rautenstrauch-Joest-Museum Cologne) with white efflorescence crystals (magenta highlighted areas). ©Anke Freud

Fig. 2. (a) Attic black figured amphora of the Antikensammlung Munich, high 54 cm, (b) view from above through the black rim into the amphora; hairy crystals growing from white deposits (magenta cycle), (c) hairy crystals growing on the outside of the amphora (magenta highlighted area) © Anton Buhl

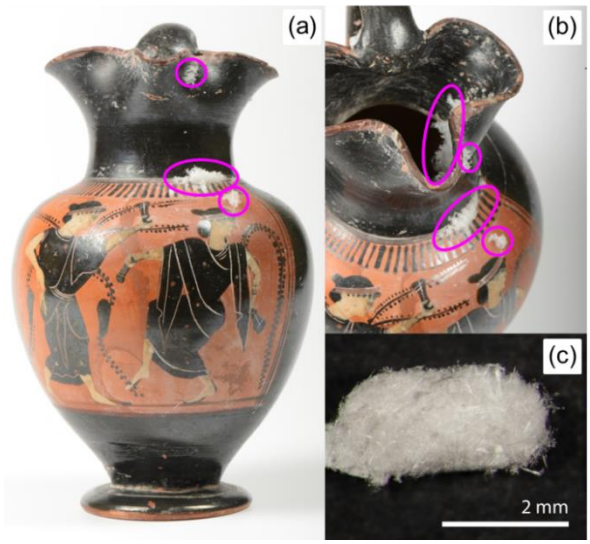

Fig. 3. (a) Black figured Attic wine jug (PC 25, height: 15.7 cm) with dancing maenads[20] ca. 500 BCE, Needle agglomerates on neck (magenta highlighted areas), (b) Detail of the samples: needle agglomerates on the neck and inside (magenta highlighted areas), (c) Microscopic view of the needle agglomerates on sample PC 25. (a) & (b) © National Museum of Antiquities Leiden, (c) © Rebekka Kuiter

Table 1.
Overview on investigated corrosion samples.

Sample notation	Sample Description	Source
Sample 52273	white efflorescence crystals grown on an Anatolian copper alloy bowl	Rautenstrauch-Joest-Museum Cologne
Sample SH-1413	white efflorescence crystals grown on a black figured Attic amphora, bought in 1831 by Ludwig I. of Bavaria from the Candelori collection	Antikensammlung Munich
Sample PC25 Sample PC26	white efflorescence crystals grown on black-figured Attic wine jugs (*oinochoai*), ca. 500 BCE	Prince of Canino Collection, in the National Museum of Antiquities Leiden (NL)

2.2.Phase Characterization

2.2.1. SEM-EDX Analysis

The white efflorescence crystals of samples 52273 and SH-1413 (Table 1) were investigated by scanning electron microscopy (SEM) and energy dispersive X-ray spectroscopy (EDX) using a Zeiss EVO 60 microprobe and an accelerating Voltage of 20 kV. For the micrographs, the samples have been sputtered with carbon.

2.2.2. Ion Chromatography

The sample 52273 (Table 1) was analysed using a protocol developed for the analysis of soluble salts occurring on the surface of historic glasses, for experimental details see[21].

2.2.3. Raman-spectroscopy

µ-Raman spectroscopy of samples 52773 and SH-1413 (Table 1) was conducted using a Renishaw inVia Raman spectrometer with a Leica DMLM microscope and a RenCam CCD detector. The spectrometer was equipped with a He-Ne laser operating at 632.8 nm, with power kept below 400 µW on the sample surface.

2.2.4. Thermal Analysis

Thermal analysis was carried out on sample SH-1413 (Table 1) using a STA 449 F5-Jupiter (Netzsch) device for TG-measurements. 2.3 mg of the sample were placed in an Al_2O_3 crucible and heated up from 30 °C to 1000 °C with a heating rate of 2 K/min in a 50 mL/min Ar-stream. An empty Al_2O_3 crucible was used as reference material. After cooling down to room temperature in an Ar-stream, the residue of the thermal decomposition was immediately transferred into a capillary, that was sealed and analysed by ex-situ X-ray powder diffraction (see below).

2.2.5. Laboratory X-ray powder diffraction

The XRPD patterns of all solids used for quantitative phase analysis and crystal structure solution were collected at room temperature on a laboratory powder diffractometer in Debye-Scherrer geometry (Stadi P-Diffraktometer (Stoe), Cu-Kα1 radiation from primary Ge(111)-Johann-type monochromator, Mythen 1 K detector (Dectris)). The samples were sealed in 0.3 mm diameter borosilicate glass capillaries (Hilgenberg glass No. 14), which were spun during the measurements. Each pattern was measured in a 2 θ range from 5.0° to 90.5° applying a total scan time of 14 h and 17 min.

2.2.6. In- and ex-situ *X-ray powder diffraction*

Temperature dependent *in situ* XRPD measurements were carried out on a laboratory powder diffractometer in Debye-Scherrer geometry (Stadi P-Diffraktometer (Stoe), Mo-Kα1 radiation from primary Ge(111)-Johann-type monochromator, array of 3 Mythen 2 K detectors (Dectris)) using sample SH-1413 (Table 1). The sample was sealed in a 0.3 mm diameter borosilicate glass capillary (Hilgenberg glass No. 14), which was spun during the measurements. The patterns were measured in a 2 θ range from

2.0° to 115.0° applying a total scan time of 30 min per measurement. The temperature was adjusted using an Oxford Cryostream device (Oxford Cryostream 500, Oxford Cryosystems). The sample was heated form 30 °C to 220 °C in steps of 5 K. During each step a diffraction pattern was collected. Afterwards the sealed capillary was cooled down to room temperature and stored for four days and then measured again using a diffractometer and scan parameters described below to check for reversibility of the decomposition process. The residue after thermal decomposition of sample SH-1413 was investigated with a similar device that is equipped with one Mythen 1 K detector (Dectris). The pattern was measured with a 2 θ range from 2.0° to 60.0° applying a total scan time of 10 h.

2.3.Structure Determination

The program TOPAS 6.0[22] was used to determine and refine the crystal structure of $Ca_2(CH_3COO)(HCOO)(NO_3)_2 \cdot 4H_2O$ using sample 52273 (Table 1). Indexing of the phase was carried out by an iterative use of singular value decomposition (LSI)[23] leading to a primitive triclinic unit cell with lattice parameters given in the Supporting Information (Table S1) and $P1$(1) or $P\bar{1}$(2) as possible space groups. The peak profile and the precise lattice parameters were determined by LeBail[24] fits applying the fundamental parameter approach of TOPAS[25]. The background was modelled by employing Chebychev polynomials of 6th order and the hump in the background caused by the glass capillary was modelled by a very broad Lorentzian shaped peak. The refinement converged quickly.

The crystal structure of $Ca_2(CH_3COO)(HCOO)(NO_3)_2 \cdot 4H_2O$ was solved by applying the global optimization method of simulated annealing (SA) in real space as it is implemented in TOPAS[26]. Crystal structure solution was carried out using both space groups, $P1$(1) and $P\bar{1}$(2). Considering the determined unit cell volume and the packing density of related compounds (see below) the content of the unit cell was estimated with 2x Ca, 4x A with A = $HCOO^-$, CH_3-COO^-, NO_3^- and *n*x H_2O. For structure solution in space group $P1$ rigid bodies for the formate ($HCOO^-$), the acetate (CH_3-COO^-) and nitrate (NO_3^-) were defined in z-matrix notation and freely translated and rotated within the unit cell. With respect to the results of the ion chromatography (see below) and the site multiplicity of $P1$, one acetate, one formate and two nitrate units were included in the simulated annealing process. The global optimization was carried out many times; including different numbers of oxygen sites, representing hydrate water. Oxygen atoms situated on identical positions were identified by using a merging radius of 0.7 Å[27]. In result the simulated annealing process always yielded identical structural models that were independent from the starting parameters and represented a phase composition of $Ca_2(CH_3COO)(HCOO)(NO_3)_2 \cdot 4H_2O$. For the final Rietveld refinement[28], all profile and lattice parameters were released iteratively and positions of the calcium and oxygen (hydrate water) atoms were subjected to free unconstrained refinement. The bond lengths and angles of the rigid bodies were refined, restraining them to reasonable values and the hydrogen positions were omitted due to the limits of the powder diffraction method. A close inspection of the atomic positions revealed a pronounced pseudo centrosymmetry which is only broken by the crystallographic non-equivalent formate-acetate pair. In order to check for centrosymmetry, crystal structure solution was carried out again using space group $P\bar{1}$. Instead of distinct rigid bodies for formate and acetate units a R-COO^- unit with R = H and CH_3 was created in z-matrix notation with refineable side occupancies for the hydrogen and the methyl rest to model an occupationally disordered acetate/formate site. This led to a similar structure model as obtained using $P1$ with occupancy factors for both acetate and formate of ≈ 0.5, thus representing a

$Ca_2(CH_3COO)(HCOO)(NO_3)_2 \cdot 4H_2O$ phase composition, as well. Due to the constitution of the anions an occupational disorder between acetate, formate and nitrate would be also possible. In order to check this, an acetate/formate rigid body was added to the position of the nitrate ion and vice versa with equally orientated anions at the same position. For the nitrate site, the site occupancy factor of the acetate/formate ion was refined to 0 and for acetate/formate site the occupancy factor of the nitrate ion was refined 0, as well. In addition an inspection of the difference Fourier map did not show any positive or negative residual electron density at the anion sites. Therefore a disorder between acetate/formate and nitrate could be excluded.

To evaluate the *P*1 structure model representing a fixed $Ca_2(CH_3COO)(HCOO)(NO_3)_2 \cdot 4H_2O$ phase composition and the $P\bar{1}$ structure model representing a variable $Ca_2(CH_3COO)_x(HCOO)_{2-x}(NO_3)_2 \cdot 4H_2O$ phase composition all samples of the white efflorescence salt (Table 1) were subjected to Rietveld refinements[28] using both structure models as starting parameters. As each sample was stored in a different way and contained a different amount of salt contamination the crystallization of the calcium acetate formate nitrate hydrate would yield different acetate : formate ratios, x, in the solid (see below) and different lattice parameters if the *P*1 structure model was not suitable. In fact all sample exhibit identical lattice parameters. In addition a Rietveld refinement using the *P*1 structure model with all atomic and thermal displacement parameters kept fixed yielded a good fit of the diffraction pattern (Supporting information, Figure S2-S4). The same procedure was carried out using the $P\bar{1}$ structure with the site occupancies of acetate and formate at the positional disordered anion site used as an additional refineable parameter. In each case the occupancy factors for both acetate and formate were refined to ≈ 0.5. Therefore the *P*1 crystal structure model with a completely ordered anion sublattice is considered as representative for the crystal structure of $Ca_2(CH_3COO)_x(HCOO)_{2-x}(NO_3)_2 \cdot 4H_2O$. The final agreement factors are listed in Table S1, the atomic coordinates and selected bond distances are given in Table S2 and Table S3, the fit of the whole powder pattern is shown in Figure S1 in the supporting information. The crystallographic data have been deposited at CCDC, deposit number: 1553033.

3. Results

3.1.Phase Identification and Characterization

3.1.1. Crystal morphology and phase composition

All white efflorescence crystals that were collected had a needle like shape that was visible with the naked eye or using an optical (Fig. 3, c) or scanning electron microscope employing a low magnification (Fig. 4, a, c, d). Some of the crystals were apparently glistening, suitable crystals for single crystal X-ray diffraction, however, could not be found in any of the samples. Scanning electron microcopy revealed that the needles are rather polycrystalline agglomerates than single crystals (Fig. 4, b). Some of the aggregates exhibit mechanical damage from sampling.

The samples 52273 and SH-1413 were subjected to a semi-quantitative EDX-analysis. For both samples calcium and oxygen were found as the main constituents (Supporting Information, Table S4). It should be noted that due to the low amount of sample and due to the limitations of the EDX-method, the given content of oxygen as a light element rather represents a rough estimate than an exact determination. In

addition the contents of carbon and nitrogen were not determined at all. For sample SH-1413 traces of sulfur, sodium and aluminum (both < 0.5 wt %) were found, as well. Sample 52273 was also analyzed by ion chromatography. Except for a trace of sodium (possibly contamination from the glass vial) only calcium was found as cation. Acetate, formate and nitrate were found as anions with a ratio of ca. 1.0 acetate : 1.0 formate : 1.5 nitrate. Crystal structure determination using sample 52273 (see above) was successfully performed using a phase composition of $Ca_2(CH_3COO)(HCOO)(NO_3)_2 \cdot 4H_2O$.

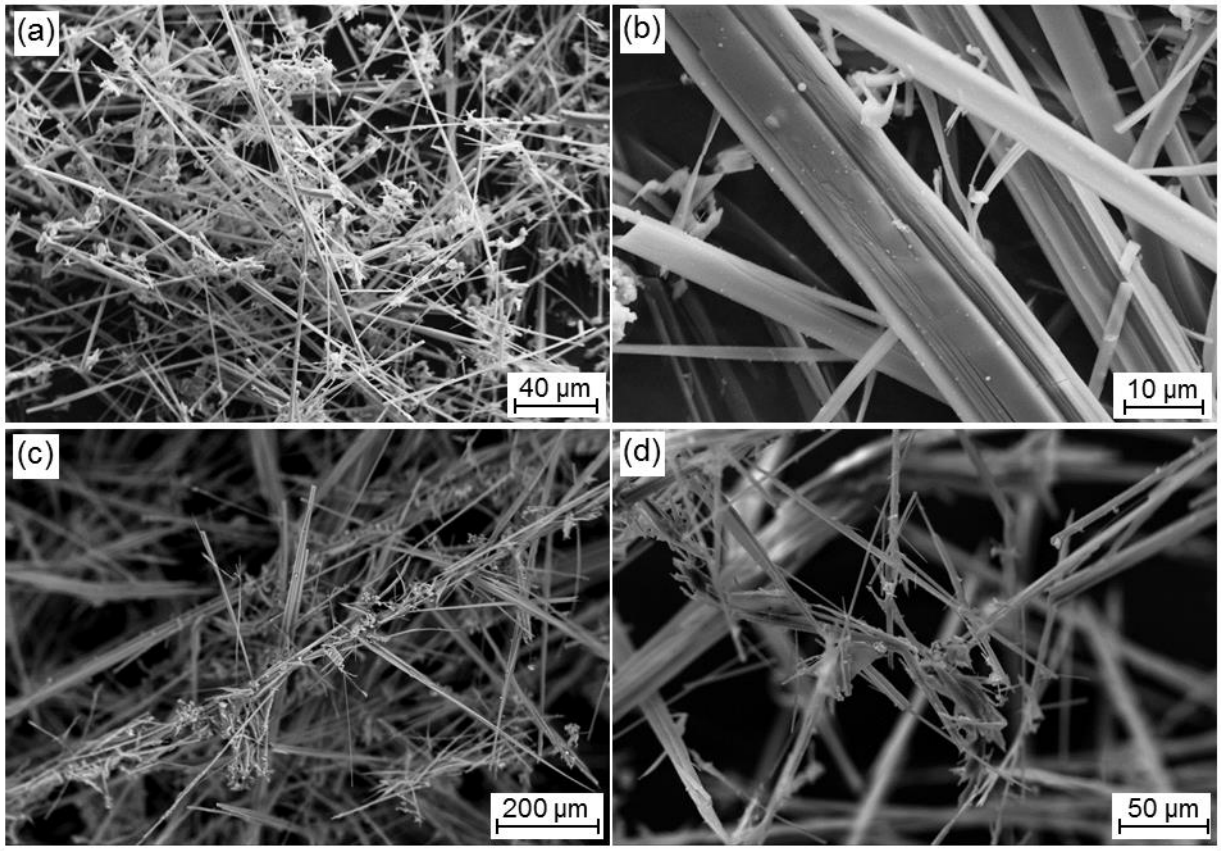

Fig. 4. SEM-images of white efflorescence crystals of sample 52273 (a), (b) and sample SH-1413 (c), (d).

3.1.2. X-ray powder diffraction

All samples of white efflorescence crystals were investigated by X-ray powder diffraction (XRPD) and the measured patterns were compared to calculated patterns of calclacite ($Ca(CH_3COO)Cl \cdot 5H_2O$)[6], $Ca_2(CH_3COO)_3NO_3 \cdot 2H_2O$[19] and thecotrichite ($Ca_3(CH_3COO)_3Cl(NO_3)_2 \cdot 6H_2O$)[8] (Fig. 5, a-c). The measured patterns are basically identical (Fig. 5, d-g) and they significantly differ from the calculated ones of the known efflorescence products. In addition, no match of the measured reflection positions to any entry in the PDF4-database[29] could be found, hence the investigated efflorescence crystals represent a hitherto unknown phase. A close inspection of the measured diffraction patterns, however, reveals slight differences. In the pattern of samples SH-1413, PC25 and PC26 an additional weak reflection is apparent at ca. 11.5°2θ (Fig. 5, e-g, star) that can be assigned to $CaSO_4 \cdot 2H_2O$ (gypsum). Sample PC26 exhibits further reflections (Fig. 5, e, triangles) that can be assigned to $CaCO_3$ (calcite) and three additional reflections (26.0, 26.6 and 27.0°2 θ, Fig. 5, squares) that cannot be assigned unambiguously to any known phase. In conclusion sample 52273 can be considered as a pure sample of a

new efflorescence product and was therefore used for crystal structure determination (see above). The other samples were subjected to a quantitative phase analysis (Supporting Information, Figure S 2-4). In result it could be demonstrated, that the structural model derived from sample 52273 is suitable for all other samples, as well. Samples SH-1413 and PC25 contain small impurities of gypsum (4.1 and 3.5 wt-% Table 2), whereas sample PC26 contains a significant amount of calcite.

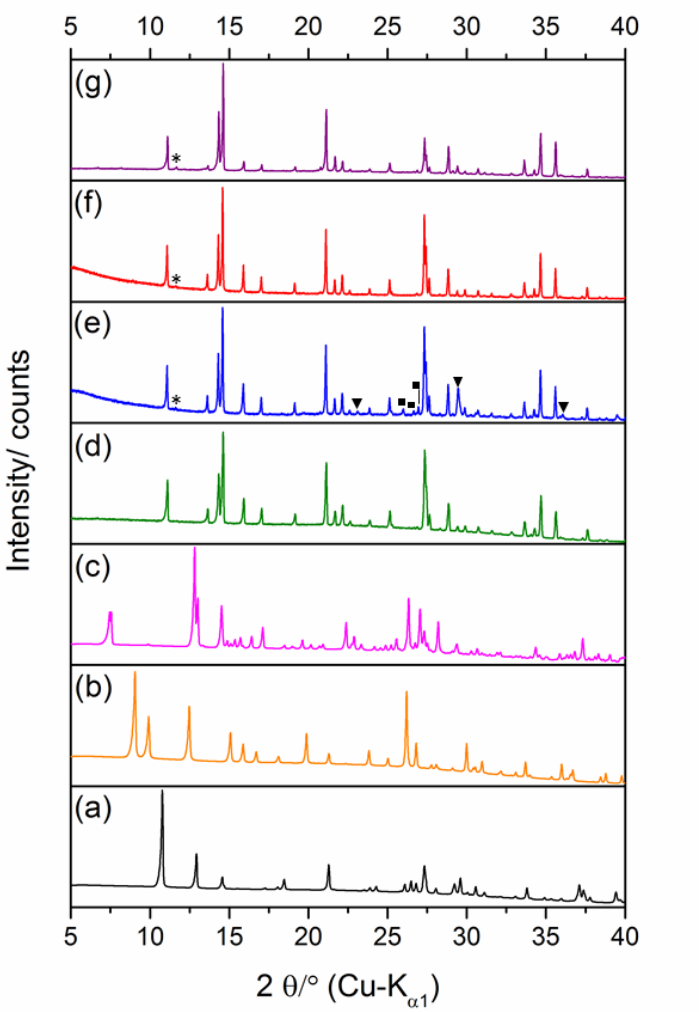

Fig. 5. Simulated XRPD patterns of (a) calclacite, (b) $Ca_2(CH_3COO)_3NO_3 \cdot 2H_2O$, (c) thecotrichite and measured XPRD pattens of sample (d) 52273, (e) PC26, (f) PC25 and (g) SH-1413. *In patterns (e-f) the presence of gypsum is indicated by the appearance of the 020 reflection. ▼In pattern (e) some reflections could be assigned to calcite, and some additional reflections ■ that cannot be assigned unambiguously.

Table 2
Crystalline components in the samples of white efflorescence crystals according to quantitative phase analysis (Supporting Information, Figure S2-S4).

Sample	**Composition according to quantitative phase analysis by XRPD**
Sample 52273	pure $Ca_2(CH_3COO)(HCOO)(NO_3)_2 \cdot 4H_2O$
Sample SH-1413	95.9 wt-% $Ca_2(CH_3COO)(HCOO)(NO_3)_2 \cdot 4H_2O$, 4.1 wt-% $CaSO_4 \cdot 2H_2O$
Sample PC25	96.5 wt-% $Ca_2(CH_3COO)(HCOO)(NO_3)_2 \cdot 4H_2O$, 3.5 wt-% $CaSO_4 \cdot 2H_2O$
Sample PC26	90.1 wt-% $Ca_2(CH_3COO)(HCOO)(NO_3)_2 \cdot 4H_2O$, 0.9 wt-% $CaSO_4 \cdot 2H_2O$ + 9.0 wt-% CaCO3 (calcite) and a trace of a non-identified phase

3.1.3. Raman Spectroscopy

The white efflorescence crystals of samples 52273 and SH-1413 were investigated by Raman spectroscopy and the measured spectra were compared to the Raman spectrum of thecotrichite ($Ca_3(CH_3COO)_3Cl(NO_3)_2 \cdot 6H_2O$). The complete spectra are presented in the Supporting Information (Figure S5), in Fig. 6 excerpts of the high- (a) and mid-Raman shift regions (b) are shown. For the band assignment (Table 3) spectroscopic data of $Ca(HCOO)_2$[30], $Ca(CH_3COO)_2 \cdot H_2O$[31], $Ca(CH_3COO)_2$[32], $Ca(NO)_3 \cdot 4H_2O$[33] as well as the fundamental vibrations of the nitrate ion[34] and the acetate ion[35] were used. The measured spectra of the two samples of $Ca_2(CH_3COO)(HCOO)(NO_3)_2 \cdot 4H_2O$ are identical in terms of band positions and the number of bands present (Fig. 6, green and violet lines). This is an additional support of the *P*1 structure model (see above) that represents a fixed phase composition with a non-variable anion ratio as complex salts having a variable phase composition exhibit differences in the band positions and sometimes in the band numbers in the vibrational spectra[36].

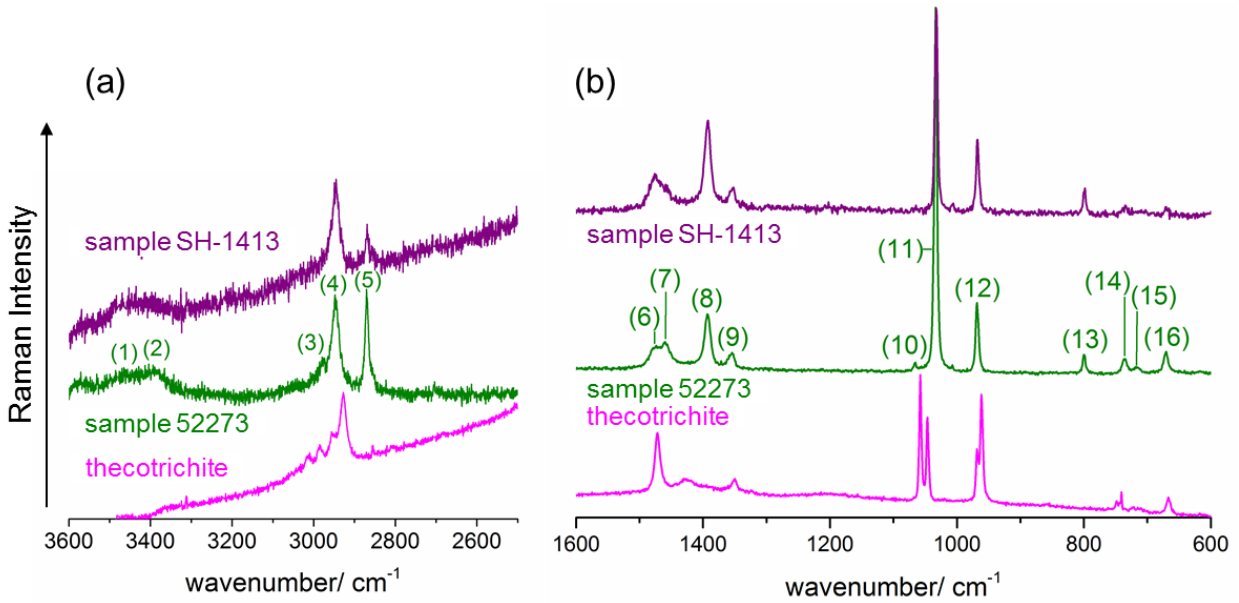

Fig. 6. Comparison of the measured Raman spectra of Thecotrichite ($Ca_3(CH_3COO)_3Cl(NO_3)_2 \cdot 6H_2O$), sample 52273 and sample SH-1413 (a) in the high- and (b) in the mid-Raman shift region, for band assignment see Table 3.

In the high-Raman shift region (Fig. 6, a) of the spectra of $Ca_2(CH_3COO)(HCOO)(NO_3)_2 \cdot 4H_2O$ at least two very broad band are visible that can be assigned to OH-stretching modes of the hydrate water molecules present in the crystal structure (Table 3, band no. (1), (2)). Like thecotrichite, $Ca_2(CH_3COO)(HCOO)(NO_3)_2 \cdot 4H_2O$ exhibits acetate related CH-stretching modes at (2925-3000) cm^{-1} (band no. (3), (4)), but an additional CH-stretching mode present in the Raman-spectra (band no. (5)) cannot be assigned to acetate ions, as it is located clearly below 2900 cm^{-1}. The occurrence of this band confirms the presence of formate ions and it can be assigned to the in-plane CH-stretching mode of the anion. Another confirmation of the presence of formate ions in the white efflorescence phase of samples 52273 and SH-1413 can be found in the region of mid-Raman shifts (Fig. 6, b). Nitrate attributed NO stretching modes are present in all spectra between 1350 cm^{-1} and 1500 cm^{-1} (Table 3, band no. (6), (7) and (9)). The spectra of samples 52273 and SH-1413 exhibit an additional, sharp band, which is related to an in-plane deformation mode of the formate ion. Other prominent features of the Raman spectrum of

$Ca_2(CH_3COO)(HCOO)(NO_3)_2 \cdot 4H_2O$ are the very sharp ν_1 stretching mode of the nitrate ions (band no. 11) and the sharp ν_4 stretching mode of the acetate ions (band no. 12), which are also present in the Raman spectrum of thecotrichite.

Table 3
Measured band positions of $Ca_2(CH_3COO)(HCOO)(NO_3)_2 \cdot 4H_2O$ (Fig. 6), band assignment according to [30–35].

band no.	band position/ cm^{-1}, shape	assignment	band no.	band position/ cm^{-1}, shape	assignment
(1)	≈3465 w, br	ν(OH) [hydrate water]	(11)	1034 vs, s	ν(NO) [nitrate]
(2)	≈3395 w, br		(12)	968 s	ν(CO) [acetate]/
(3)	2978 w, br	ν(CH) [acetate]	(13)	800 s	γ(CO) [formate]
(4)	2947 m		(14)	736 m	ν(NO) [Nitrate]
(5)	2871 s	ν(CH, in plane) [formate]	(15)	717 w, br	γ(OH) [hydrate water]
(6)	1475 m, br	ν(NO) [nitrate]	(16)	670 m	ν(CO) [acetate]
(7)	1458 m				
(8)	1393 s	γ(CH, in plane) [formate]	(17)	≈190 m, br	
(9)	1355 m	ν(CO) [formate]/ ν(NO) [nitrate]	(18)	≈140 m, br	lattice vibrations
(10)	1067 s	ν(CH, out of plane) [formate]	(19)	117 s	

vs = very strong, m = medium, w = weak, br = broad, s = sharp

3.2.Thermal Decomposition

The thermal behaviour of $Ca_2(CH_3COO)(HCOO)(NO_3)_2 \cdot 4H_2O$ was studied by thermogravimetric analysis covering a temperature range from 30 °C to 1000 °C, *ex-situ* XRPD of the residue after the thermal analysis and temperature dependent *in-situ* XRPD measurements in a sealed capillary covering a temperature range from 30 °C to 220 °C in which hydrate water is released. In order to check the dehydration reaction for reversibility the capillary of the *in-situ* XRPD measurements was cooled down to room temperature, stored for four days and measured again by XRPD.

3.2.1. Thermal Analysis

Thermal decomposition of $Ca_2(CH_3COO)(HCOO)(NO_3)_2 \cdot 4H_2O$ in a dry Ar-gas stream starts at ca. 60 °C , ends at ca. 710 °C and proceeds as a 4-step process (Fig. 7). The first two steps of the decomposition process overlap (Fig. 7, inset). As the second decomposition step already ends at ca. 140 °C, these steps are most likely associated with the release of hydrate water. The step height of the first two steps is almost equal; hence it can be assumed that in each step two molecules of hydrate water are released. There is a slight derivation of the measured (21.1 wt-%) to the calculated total mass loss (19.0 wt-%) of the first two steps (Table 4), which is attributed to adsorbed water as the efflorescence crystals are hygroscopic and to gypsum, which is present as a small impurity (Table 2). The next decomposition step takes place between 325 °C and 375 °C. According to the measured mass loss, $Ca_2(CH_3COO)(HCOO)(NO_3)_2$ is completely decomposed into $CaCO_3$ (Table 4). This is seemingly in contradiction to the decomposition mechanism of $Ca(NO_3)_2 \cdot 4H_2O$[37], which first releases all hydrate water molecules upon heating and the decomposition

of the nitrate ions above 500 °C yields CaO. The thermal decomposition of carboxylate salts, i.e. acetate and formate which takes place at ca. 380°C ($Ca(CH_3COO)_2$)[38] and 360°C $Ca(HCOO)_2$[10], however leads to the formation of reactive radical species[39] that react with the nitrate ions and lead to the conversion of $Ca_2(CH_3COO)(HCOO)(NO_3)_2$ into $CaCO_3$. During the last decomposition step the solid is decomposed into CaO, which was confirmed by *ex-situ* XRPD analysis of the residue (Supporting Information, Figure S6.). The measured total mass loss (70.8 wt-%) is in good according with the calculated value (70.5 wt-%).

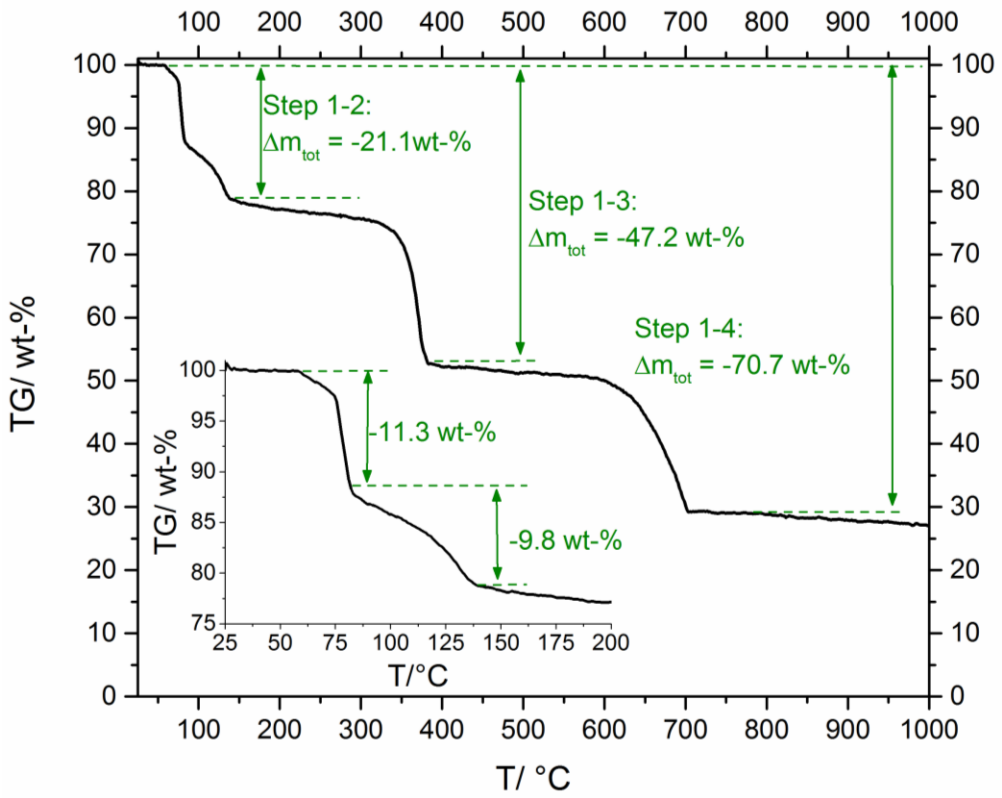

Fig. 7. Thermal analysis of $Ca_2(CH_3COO)(HCOO)(NO_3)_2 \cdot 4H_2O$.

Table 4
Assignment of the observed decomposition steps in the TG-curve.

steps	Reaction/ residue	total mass loss/ wt-%	
		calc.	meas.
(1)	release of ≈ 2.0 mol* hydrate water		
(2)	release of ≈ 2.0 mol* hydrate water	19.0	21.1
(1)-(2)	residue: $Ca_2(CH_3COO)(HCOO)(NO_3)_2$		
(3)	decomposition of the acetate, formate and nitrate ions residue: 2 $CaCO_3$	47.4	47.2
(4)	decomposition of the carbonate ions residue: 2 CaO	70.5	70.8

*estimated from the ratio of step sizes in the TG-curve (**Error! Reference source not found.**, inset)

3.2.2. In- and Ex-situ *X-ray powder diffraction*

In-situ XRPD measurements revealed the occurrence of four different crystalline phases during the thermal dehydration of $Ca_2(CH_3COO)(HCOO)(NO_3)_2 \cdot 4H_2O$ between 30°C and 220°C (Fig. 8). During this experiment the decomposition of the white efflorescence phase occurred at slightly higher temperatures than observed during the thermal analysis (atmosphere: dry Ar-gas stream), as the measurements were carried out in a sealed capillary. With respect to the TG-curve (Fig. 7) XRPD patterns of the first crystalline decomposition product that were measured between 90 and 130°C (Fig. 8, b) can be assigned to $Ca_2(CH_3COO)(HCOO)(NO_3)_2 \cdot 2H_2O$. According to the thermal analysis the decomposition of the dihydrate phase into $Ca_2(CH_3COO)(HCOO)(NO_3)_2$ occurs as a one-step process (Fig. 7), in the in-situ XRPD patterns, however, the occurrence of a short-lived crystalline intermediate can be observed (Fig. 8, c, d). This intermediate could be a sub-hydrate, $Ca_2(CH_3COO)(HCOO)(NO_3)_2 \cdot xH_2O$ with $x < 2.0$ or a second polymorph of $Ca_2(CH_3COO)(HCOO)(NO_3)_2$. Due to the pronounced polymorphism of anhydrous Calcium acetate[11] and –formate[9] the occurrence of an α- and β- form of $Ca_2(CH_3COO)(HCOO)(NO_3)_2$ would not be unexpected.

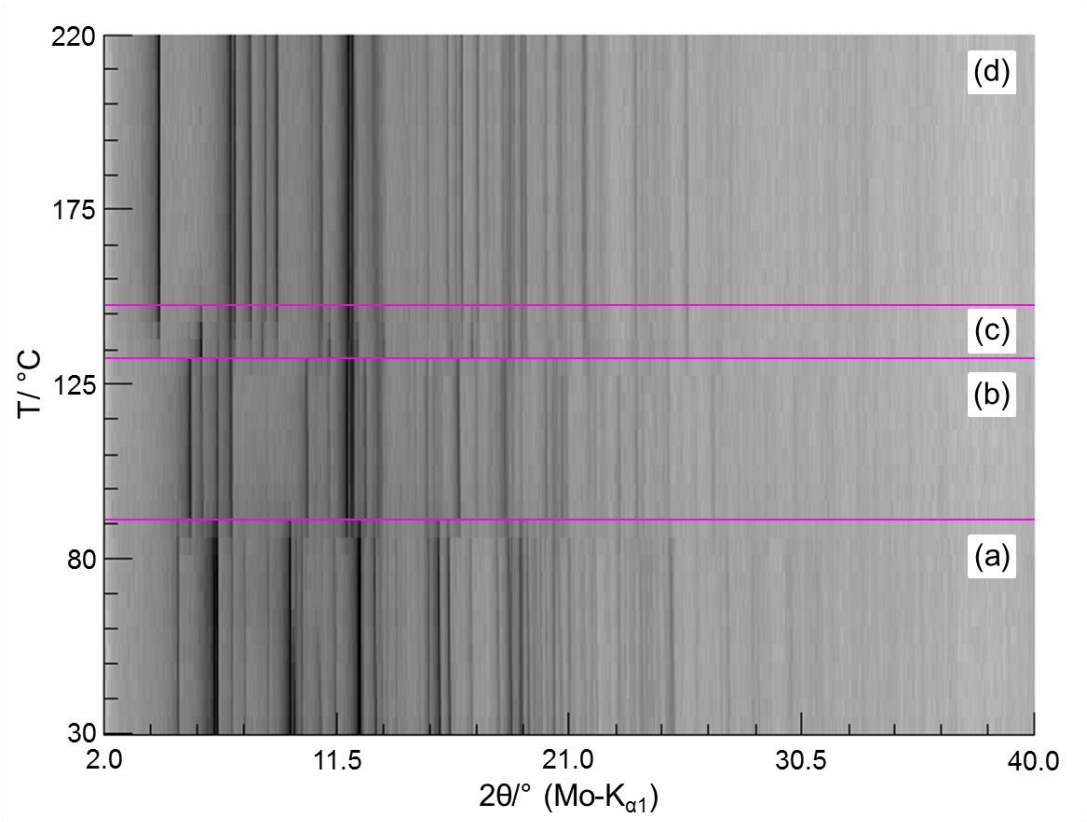

Fig. 8. Temperature dependent *in-situ* XRPD measurements (MoKα1 radiation, 0.7093 Å) of $Ca_2(CH_3COO)(HCOO)(NO_3)_2 \cdot 4H_2O$ (a) starting material, (b) $Ca_2(CH_3COO)(HCOO)(NO_3)_2 \cdot 2H_2O$ (c) α-$Ca_2(CH_3COO)(HCOO)(NO_3)_2$ or $Ca_2(CH_3COO)(HCOO)(NO_3)_2 \cdot xH_2O$ with $x < 2.0$, (d) ß-$Ca_2(CH_3COO)(HCOO)(NO_3)_2$.

The final product of the dehydration reaction (Fig. 8, d) was cooled down to room temperature and stored for four days to check for a rehydration of $Ca_2(CH_3COO)(HCOO)(NO_3)_2$ in the water vapor saturated atmosphere of the capillary. A comparison of the measured powder patterns of the starting material, the

intermediates and the product of the *de*hydration reaction with product of the *re*hydration is presented in Fig. 9. It is obvious that $Ca_2(CH_3COO)(HCOO)(NO_3)_2$ (Fig. 9, d) was rehydrated to a mixture of $Ca_2(CH_3COO)(HCOO)(NO_3)_2{\cdot}2H_2O$ (Fig. 9, e, stars) and $Ca_2(CH_3COO)(HCOO)(NO_3)_2 \cdot 2H_2O$ (triangles). A complete rehydration, however, seems to be slow, as the reaction is not completed after four days.

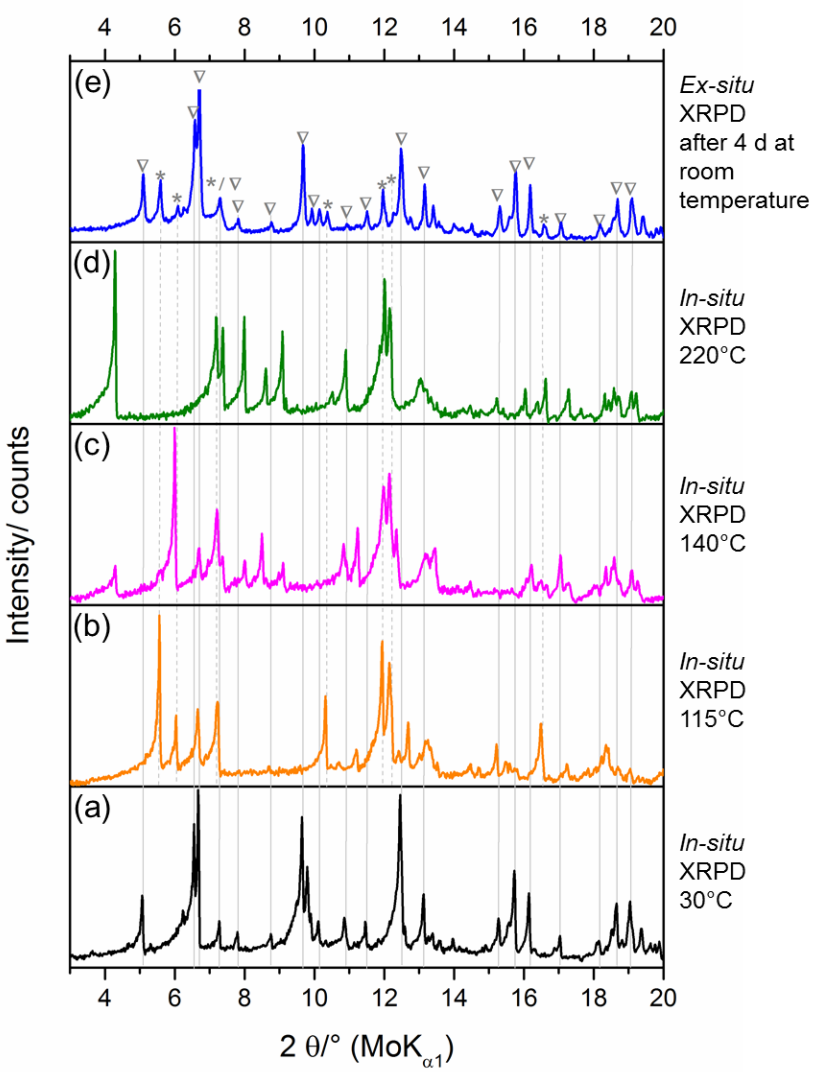

Fig. 9. XRPD patterns of (a) $Ca_2(CH_3COO)(HCOO)(NO_3)_2{\cdot}4H_2O$ at 30°C, (b) $Ca_2(CH_3COO)(HCOO)(NO_3)_2{\cdot}2H_2O$ at 115°C (c) α-$Ca_2(CH_3COO)(HCOO)(NO_3)_2$ or $Ca_2(CH_3COO)(HCOO)(NO_3)_2{\cdot}xH_2O$ with $x < 2.0$ at 140°C, (d) ß-$Ca_2(CH_3COO)(HCOO)(NO_3)_2$ at 220°C (all *in-situ* data of heating a sealed capillary) and (e) rehydration of ß-$Ca_2(CH_3COO)(HCOO)(NO_3)_2$ in the sealed capillary yielding a mixture of $Ca_2(CH_3COO)(HCOO)(NO_3)_2{\cdot}2H_2O$ (*) and $Ca_2(CH_3COO)(HCOO)(NO_3)_2{\cdot}4H_2O$ (▽).

3.3.Crystal Structure Description

$Ca_2(CH_3COO)(HCOO)(NO_3)_2{\cdot}4H_2O$ crystallizes in a non-centrosymmetric, primitive, triclinic lattice that contains two calcium sites. Each calcium cation is coordinated by 8 oxygen atoms from which two of each are donated by acetate-, formate-, nitrate ions and water molecules. The distances between oxygen

and calcium were determined to range between 2.15 Å and 2.64 Å (Supporting Information, Table S2), which is comparable to related compounds[6,8,19]. All oxygen atoms are located within the coordination sphere of Calcium. One calcium site is coordinated by bidentate nitrate (μ_2-NO_3) and formate (μ_2-HCOO), monodentate acetate (μ_1-CH_3-COO) and two water molecules (Fig. 10). The other calcium site exhibits an almost identical coordination sphere with bidentate acetate (μ_2-CH_3-COO) and monodentate formate (μ_1-HCOO). The CaO_8-polyhedra are bridged by carboxylate ions whereas the water molecules and the non-coordinating nitrate-oxygen are apical.

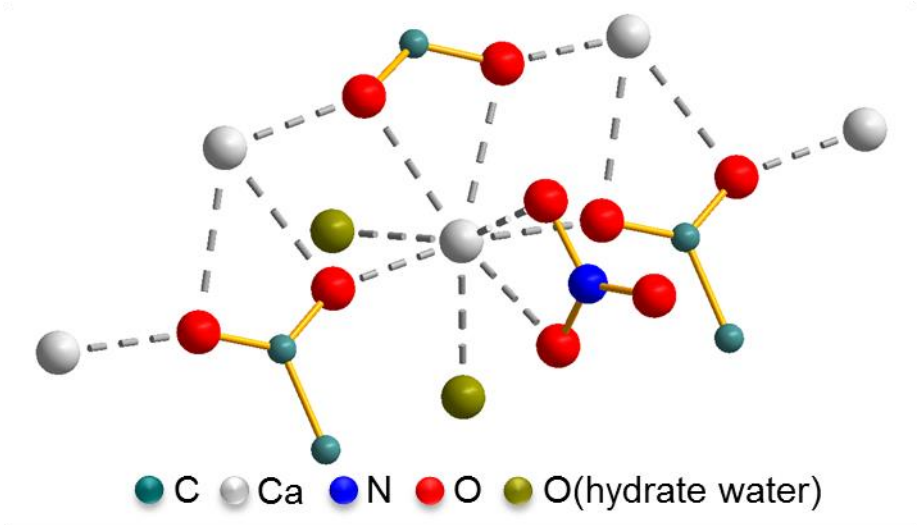

Fig. 10. Coordination spheres of cations and anions in the crystal structure of $Ca_2(CH_3COO)(HCOO)(NO_3)_2 \cdot 4H_2O$. Hydrogen positions were not determined.

The CaO_8-polyherdra form infinite zig-zag chains running in *a*-direction (Fig. 11) in which the two distinct Ca-sites are repeated alternatingly. The space in-between the chain is filled by the methyl groups of the acetate ions and the non-coordinating oxygen atoms of the nitrate ion. Comparatively short distances between water molecules (dO(H_2O)-O(H_2O) = 2.73(2) Å) and water molecules and nitrate ions (dO(H_2O)-O(NO_3) = 3.04(1) Å) of adjacent chains point to strong dipolar interactions or even H-bonds that mediate the interconnections between the CaO_8-polyherdra chains. Due to the limits of the XRPD method, however, no attempt was made to determine or refine the hydrogen positions. Although a 7-fold coordination of calcium is present in carboxylate salts like formates[40,41] and acetate hydrates[13–15] the removal of water molecules from $Ca_2(CH_3COO)(HCOO)(NO_3)_2 \cdot 4H_2O$ by heating seems to induce vast but reversible structural changes (Fig. 9) that will be subject of a separate study.

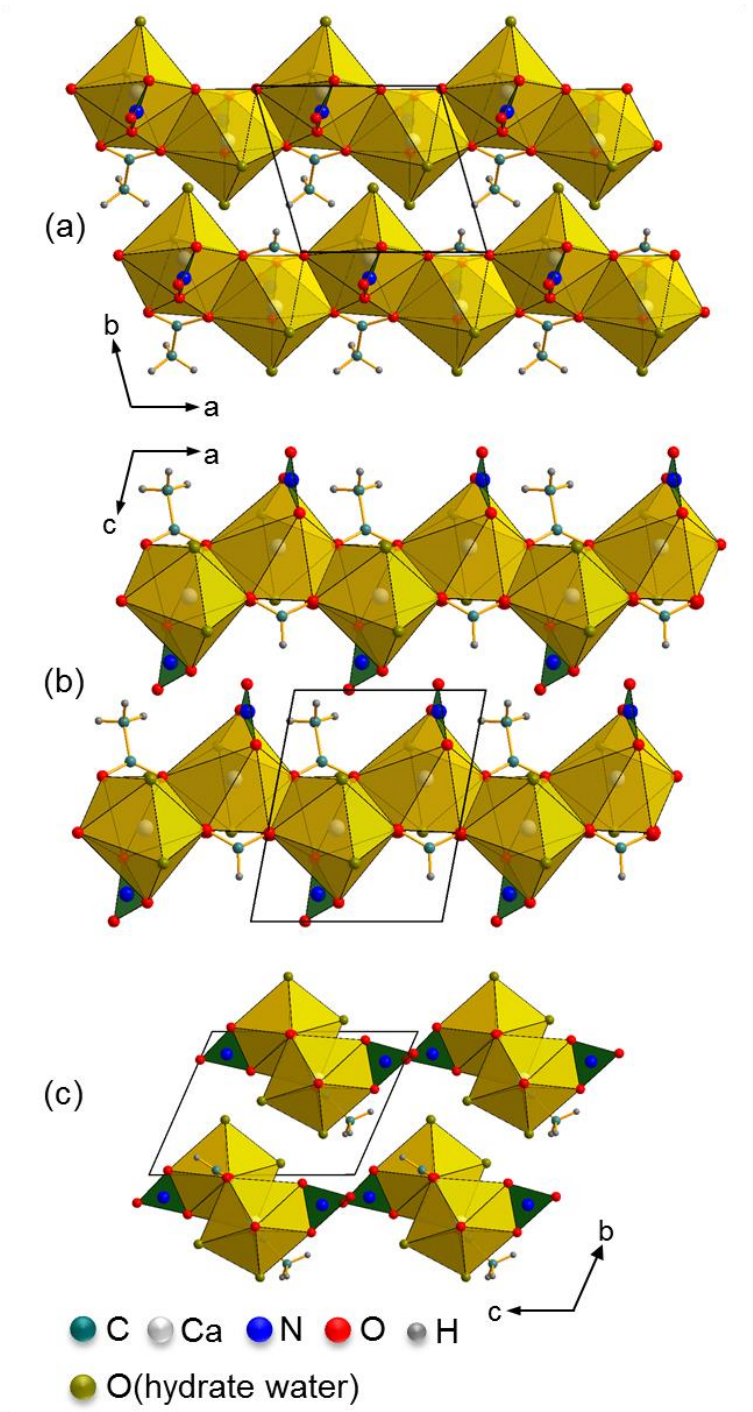

Fig. 11. Packing diagram of $Ca_2(CH_3COO)(HCOO)(NO_3)_2 \cdot 4H_2O$, views along (a) *c*-, (b) *b*- and (c) *a*-direction. CaO_8-polyhedra are displayed in yellow, nitrate ions by green triangles. Hydrogen positions were not determined. Hydrogen atoms were added to idealized positions to the acetate and formate ions for a clear distinction between them.

4. Discussion

4.1.The formation of $Ca_2(CH_3COO)(HCOO)(NO_3)_2{\cdot}4H_2O$ on calcareous heritage objects.

The ceramics were stored in collections for nearly two centuries. For such objects, the treatment on the excavation site and later in the museums is nearly never documented. On the other hand, corrosion products can give indications which chemicals have interacted with the objects during storage and cleaning and, therefore, give hints to the conservation history.

The occurrence of soluble calcium acetates is a major concern for conservation. With fluctuating relative humidity, solution and crystallization processes in the pores of the ceramic body may cause considerable salt damage. Aqueous desalination (with prior consolidation, if necessary) is mandatory.

4.1.1. Source of acetate and formate

Pollutants like acetic and formic acid or their precursors acetaldehyde and formaldehyde are interacting with heritage objects, a major source is wood or wooden products. On glass surfaces, formates dominate[21]. Consequently, on metals in contact with glass mainly formates are found, most frequent in glass-induced metal corrosion is a sodium copper formate[42]. On calcareous objects, however, acetates dominate in deterioration products. Mixed calcium acetate formates (of unknown structure) have only been reported from mollusks[12]. Here we show for the first time that formate compounds can also form on calcareous accretions on ceramics and bronze.

4.1.2. Source of nitrate

Nitrate can be formed in the soil by nitrifying bacteria but is very mobile. Therefore, it is rarely detected in the soluble salts on ceramics from semi-arid climates. A more likely source of nitrates is cleaning with nitric acid, which is not totally uncommon in ceramics conservation[43]: 'Encrustations of calcium carbonate or calcium sulphate …can be removed using acids. The acids most commonly used are hydrochloric acid and nitric acid and the organic acids oxalic acid, citric acid and acetic acid...Sulphate deposits require stronger acid solutions for removal. Some writers recommend concentrated nitric or hydrochloric acid whilst others suggest 20% nitric acid.' (p.89/91). If not thoroughly soaked in water this leaves calcium nitrate in the ceramic body reacting over time with traces of acetic and formic acid to the title compound. Therefore, the use of mineral acids should be completely avoided at all nowadays. If this is not feasible under exceptionable circumstances, their use has to be followed by thorough aqueous desalination.

4.2.Crystal chemistry of white efflorescence products and related salts

Naturally occurring efflorescence salts, calclacite ($Ca(CH_3COO)Cl{\cdot}5H_2O$), thecotrichite ($Ca_3(CH_3COO)_3Cl(NO_3)_2{\cdot}6H_2O$) and $Ca_2(CH_3COO)(HCOO)(NO_3)_2{\cdot}4H_2O$, as well as synthetic compounds, e.g. $Ca_2(CH_3COO)_3NO_3{\cdot}2H_2O$ exhibit structural similarities: I. in all crystal structures calcium is coordinated by 8 oxygen atoms forming polyhedra with a mono-capped bipyramidal shape and II all crystal structures exhibit one dimensional polymeric Ca-carboxylate ($(Ca(\mu_2\text{-R-COO}))_n$) zig zag

chains (Fig. 12). Each link of the chain is connected to neighbouring links by monodentate coordinating carboxylate ions. Thus four out of eight places in the coordination sphere of calcium are occupied by carboxylate ions forming the one dimensional polymeric backbone that is closely related to the main motif of the crystal structure of β-$Ca(HCOO)_2$[41]. Therefore crystal structures of the efflorescence salts only differ in the occupation of the four remaining ligand positions (Fig. 12, L_1-L_4) and in the occupation of voids in-between these chains.

In the crystal structure of calclacite ($Ca(CH_3COO)Cl{\cdot}5H_2O$) all ligand positions from L_1 to L_4 are occupied by apical hydrate water (Table 5) resulting in the formation of loosely packed (26.73 Å³ per non-H atom of the polymeric chains) one dimensional $[Ca(\mu_2\text{-}CH_3\text{-}COO)(H_2O)_4]^+_n$ polymeric chains (Fig. 13, a). One water molecule and one chloride ion per calcium ions are intercalated in between the chains resulting into a total packing density of 21.87 Å³ per non-H atom. In the polymeric calcium carboxylate backbone of $Ca_2(CH_3COO)(HCOO)(NO_3)_2{\cdot}4H_2O$ half of the acetate ions are replaced by formate and half of the water molecules are replaced by a bidentate coordinating nitrate ion (Fig. 13, b). In consequence charge balance is already maintained within the $[(Ca(\mu_2\text{-}CH_3\text{-}COO)(\mu_2\text{-}NO_3)(H_2O)_2)\text{-}(Ca(\mu_2\text{-}HCOO)(\mu_2\text{-}NO_3)(H_2O)_2)]_n$ polymeric chain. The space in-between the chains is filled by non-coordinating oxygen of the nitrate ions and by methyl groups of the acetate ions, which results in a high packing density (17.14 Å³ per non-H atom). Therefore neither water molecules nor halide ions are intercalated. In the polymeric backbone of $Ca_2(CH_3COO)_3NO_3{\cdot}2H_2O$ an additional water molecule is replaced by a monodentate coordinating acetate ion (Table 5). In contrast to $Ca_2(CH_3COO)(HCOO)(NO_3)_2{\cdot}4H_2O$ (Fig. 13, b) the nitrate ion and the additional acetate ion act as bridging ligands that connect the one dimensional calcium carboxylate polymeric chain with neighbouring chains (c) forming a closed packed 3-dimensional network with a packing density of 17.81 Å³ per non-H atom. Accordingly no additional molecules or ions are intercalated. The polymeric backbone of thecotrichite ($Ca_3(CH_3COO)_3Cl(NO_3)_2{\cdot}6H_2O$) (Fig. 13, d) exhibits similarities to the polymeric calcium carboxylate chain in $Ca_2(CH_3COO)(HCOO)(NO_3)_2{\cdot}4H_2O$ (Fig. 13, b). In the coordination spheres of the calcium ions in thecotrichite, two water molecules are also replaced by bidentate coordinating nitrate ions, but one third of the calcium ions (site Ca(1)) is coordinated by an additional monodentate coordinating nitrate ion, that replaces a water molecule. In contrast to $Ca_2(CH_3COO)(HCOO)(NO_3)_2{\cdot}4H_2O$ all oxygen atoms of the nitrate ions of thecotrichite are situated within the coordination sphere of calcium. Hence the nitrate ions connect neighbouring polymeric chains forming a 3d-network that is much less dense packed (packing density of 19.84 Å³ per non-H atom of the polymeric chains) than in $Ca_2(CH_3COO)_3NO_3{\cdot}2H_2O$. Due to intercalation of water molecules and chloride ions in-between the chains of thecotrichite the charge balance is maintained as well as a total packing density (18.51 Å³ per non-H atom) that is comparable with other efflorescence salts.

In summary all discussed efflorescence salt phases seem to belong to an entire structure family of one dimensional, polymeric calcium carboxylates. According to the variability of the 8-fold coordination sphere of calcium a huge variety of phases with a distinct composition in terms of the content of hydrate water, carboxylate and other anions and of intercalated ions and molecules can be expected. Thus reinvestigation of white efflorescence salts on calcareous objects or a systematic investigation on synthetic calcium carboxylate salts appears to be worthwhile.

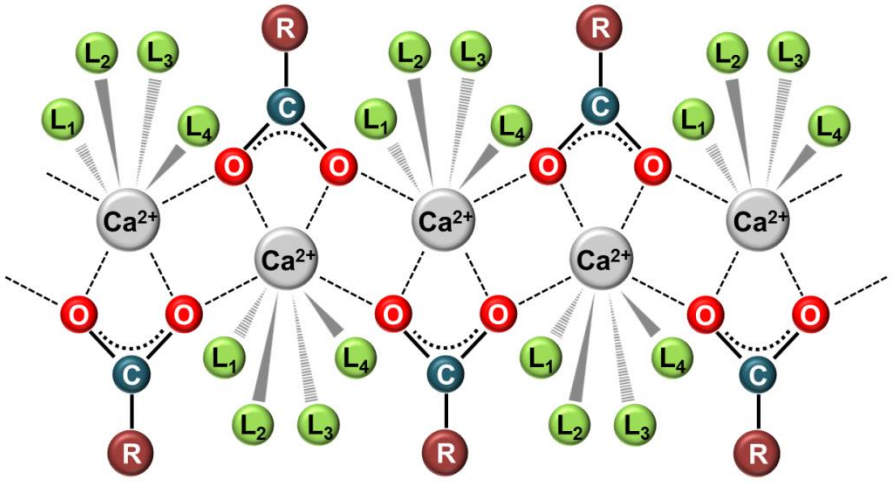

Fig. 12. One dimensional, polymeric calcium carboxylate backbone of related calcium acetate formate nitrates hydrate phases with R = H, CH_3 and L = H_2O, μ_1/μ_2-NO_3 and R-COO.

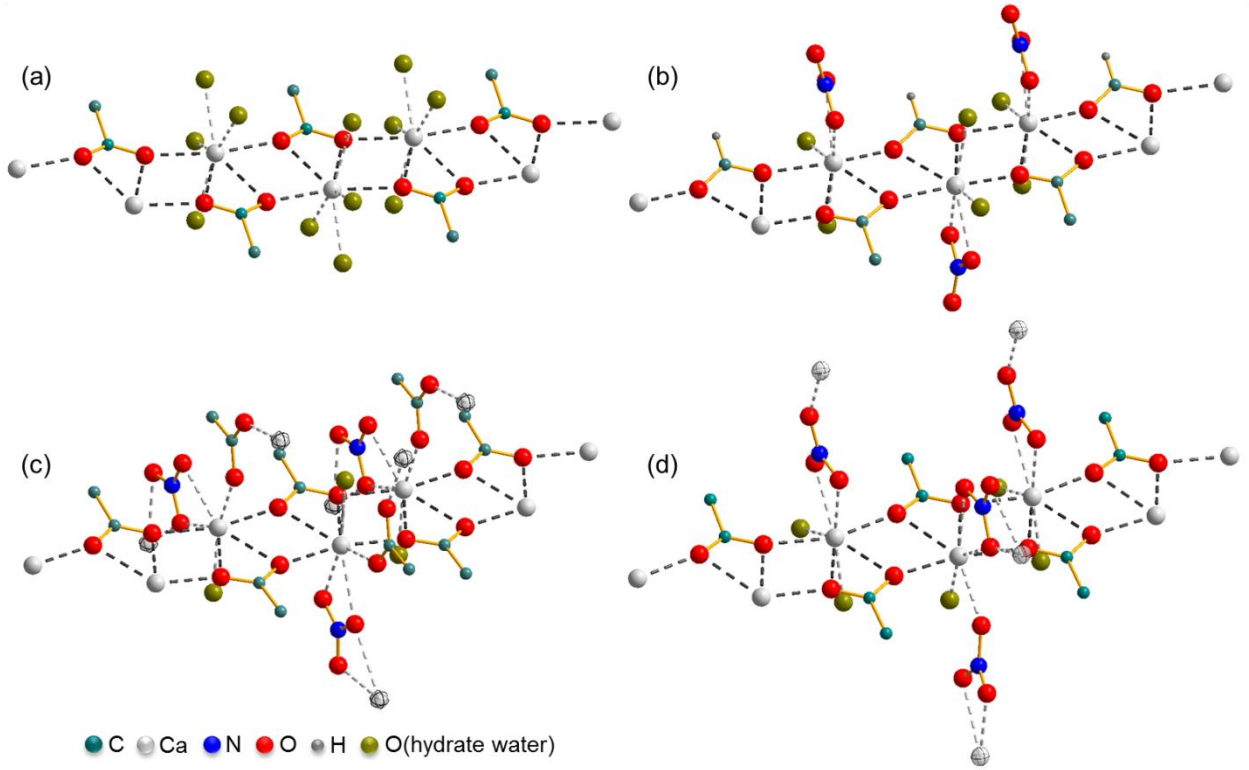

Fig. 13. Comparison of the polymeric calcium carboxylate backbones of (a) calclacite ($Ca(CH_3COO)Cl·5H_2O$), (b) $Ca_2(CH_3COO)(HCOO)(NO_3)_2·4H_2O$, (c) $Ca_2(CH_3COO)_3NO_3·2H_2O$ (the structural disorder is not explicitly shown) and (d) thecotrichite ($Ca_3(CH_3COO)_3Cl(NO_3)_2·6H_2O$).

Table 5
Comparison of polymeric calcium carboxylate backbones and structural motifs of related efflorescence salts.

name	Calclacite	-	-	Thecotrichite
formula	$Ca(CH_3COO)Cl\cdot 5H_2O$	$Ca_2(CH_3COO)(HCOO)(NO_3)_2\cdot 4H_2O$	$Ca_2(CH_3COO)_3NO_3\cdot 2H_2O$	$Ca_3(CH_3COO)_3Cl(NO_3)_2\cdot 6H_2O$
illustration	Fig. 13 (a)	Fig. 13 (b)	Fig. 13 (c)	Fig. 13 (d)
carboxylate backbone	$(Ca(CH_3COO))^+_n$	$(Ca(CH_3COO)\text{-}Ca(HCOO))^{2+}_n$	$(Ca(CH_3COO))^+_n$	$(Ca(CH_3COO))^+_n$
n H_2O : n Ca^{2+}	5	2	1	2
L_1	H_2O	H_2O	H_2O	H_2O
L_2	H_2O	} μ_2-NO_3^-	} μ_2-NO_3^-	} μ_2-NO_3^-
L_3	H_2O			
L_4	H_2O	H_2O	μ_1-CH_3COO^-	1x μ_1-NO_3^-/ 2x H_2O
structural motif	isolated 1D Ca-carboxylate chains		3D network of inter-connected 1D Ca-carboxylate chains	
intercalated ions/molecules per mol Ca^{2+}	1 H_2O, 1 Cl^-	-	-	⅓ H_2O, ⅓ Cl^-

4.3.Synopsis in a corrosion science related context

In the current study we present the identification and structural characterization of a hitherto unknown corrosion product. With their ground-breaking study on the crystal structure of β-$Fe_2Cl(OH)_3$ Réguer et al.[44] demonstrated how crystal structure data can be used to understand primary corrosion phenomena of heritage objects and secondary degradation that takes place after the excavation. These results promoted the understanding of the corrosion of state-of-the-art steel[45] and the developments of protections strategies for underwater cultural heritage[46]. The elucidated phase composition and crystal structure of $Ca_2(CH_3COO)(HCOO)(NO_3)_2\cdot 4H_2O$ can be used in the same way.

4.3.1. Conclusions on the corrosion mechanism of calcareous heritage objects

The identification of $Ca_2(CH_3COO)(HCOO)(NO_3)_2\cdot 4H_2O$ as an efflorescence salt besides calclacite ($Ca(CH_3COO)Cl\cdot 5H_2O$) and thecotrichite $Ca_3(CH_3COO)_3Cl(NO_3)_2\cdot 6H_2O$ demonstrates that efflorescence of calcareous objects in a halogenide-free environment not necessarily leads to the formation of pure Calcium acetate hydrates or calcium formates. $Ca_2(CH_3COO)(HCOO)(NO_3)_2\cdot 4H_2O$ was found on four different objects from three different museums and collections, where they were stored under different conditions. This points to a quick and easy crystallization and to a very extended crystallization field of this phase, which is similar to thecotrichite[18]. This will be subject to a subsequent study. In the crystal structure of $Ca_2(CH_3COO)(HCOO)(NO_3)_2\cdot 4H_2O$ 50 % of the carboxylate backbone consist of formate ions, despite most hard- and softwoods emit 3-10 times more acetic acid than formic acid[1]. Hence aggression by formic acid happens to much higher extent than aggression by acetic acid, which can be explained by the higher strength of formic acid.

4.3.2. Consequences for the conservation efforts of calcareous heritage objects

Due to its needle like morphology, $Ca_2(CH_3COO)(HCOO)(NO_3)_2{\cdot}4H_2O$ can be easily misidentified as thecotrichite by optical inspection or microscopy, a mistake that happened to us, as well. Accordingly museums and collection should use Raman-spectroscopy or XRPD for the diagnoses of the alteration state of calcareous heritage objects, where it is essential to identify the corrosion products unambiguously. For conservation of these objects careful dechloridation is not sufficient as halogenide ions are no essential element of the crystal structures of the efflorescence phases. Moreover, complete desalination, i.e. complete removal of halogenides and nitrates, doesn't necessarily prevent the occurrence of efflorescence salts, as calcium (from calcite) and carboxylates (from emitted formic and acetic acid) are the only essential components of the relating crystal structures. The voids in the coordination sphere of calcium can be filled with water or additional anions that are present. Careful control of the atmosphere in the storage and exhibition room is therefore essential for the conservation of calcareous historic objects. In consequence for modern preventive conservation, wood should be outlawed for permanent storage and display of ceramics. Efflorescence salts often crystallize in pores or cracks and their crystallization can cause significant damage to the artefacts[4]. $Ca_2(CH_3COO)(HCOO)(NO_3)_2{\cdot}4H_2O$ can be easily dehydrated by dry air, e.g. in heat an arid atmosphere or by heat, e.g. from spots in the exhibition room that aren't equipped with LEDs. Dehydration, i.e. the formation of $Ca_2(CH_3COO)(HCOO)(NO_3)_2{\cdot}2H_2O$ leads to a shrinking of the crystals. When $Ca_2(CH_3COO)(HCOO)(NO_3)_2{\cdot}2H_2O$ is rehydrated in humid climate or when the spots in the exhibition room are switched off, the crystals grow, again. These recrystallization processes induce a hydration pressure that leads to further degradation of the calcareous object. Accordingly both the temperature and the relative humidity must be carefully controlled in the storage and exhibition rooms.

5. Conclusion

A new white, needle like efflorescence salt was found on four different historic art objects. XRPD analyses confirmed that in each case the same, unknown compound crystallized. By EDX- and thermal analyses, as well as by ion chromatography and by Raman spectroscopy the efflorescence salt was identified as a calcium acetate formate nitrate hydrate. One of the samples was found to contain the efflorescence phase without any impurities and was therefore used for crystal structure solution from XRPD data. The obtained structural model represents a phase composition of $Ca_2(CH_3COO)(HCOO)(NO_3)_2{\cdot}4H_2O$ which was also confirmed by complementary analyses. $Ca_2(CH_3COO)(HCOO)(NO_3)_2{\cdot}4H_2O$ was found to crystallize in a non-centrosymmetric triclinic lattice with space group *P*1. The crystal structure consists of separated, one dimensional calcium carboxylate zig zag chains in which acetate and formate ions are arranged in a completely ordered alternating fashion. The coordination sphere of calcium is filled up by bidentate coordinating nitrate ions and apical water molecules. By Rietveld based quantitative phase analyses the structural model obtained from the pure sample, was found to be suitable for all investigated samples of the white efflorescence product. Thermal analysis and temperature dependent *in-situ* X-ray powder diffraction revealed that hydrate water molecules can be easily removed from $Ca_2(CH_3COO)(HCOO)(NO_3)_2{\cdot}4H_2O$ by heat or dry air, but the process was found to be reversible. The one dimensional calcium carboxylate polymeric chain as the overall structural motif of $Ca_2(CH_3COO)(HCOO)(NO_3)_2{\cdot}4H_2O$ is identical to motifs of other naturally

occurring or artificial efflorescence salts like thecotrichite, calclacite or $Ca_2(CH_3COO)_3NO_3 \cdot 2H_2O$. Thus the existence of further calcium carboxylate based efflorescence salts can be expected. The presented structural and spectral data of $Ca_2(CH_3COO)(HCOO)(NO_3)_2 \cdot 4H_2O$ can be used as the basis for an easy identification and quantitative analysis of the white efflorescence salt especially in museums and art collections worldwide.

Acknowledgement

Mrs. Christine Stefani from the Max-Planck-Institute for Solid State Research is acknowledged for performing the XRPD measurements for structure determination and Guus Verhaar from University of Amsterdam for the ion chromatography analysis. Anke Freund (Cologne) drew our attention to the bronze bowl. Renske Dooijes (National Museum of Antiquities Leiden) detected and sampled the wine jugs in her collection, Anton Buhl (Antikensammlung München) the classical ceramic.

Funding by DFG for the project „In search of structure“ (grant EG 137/9-1) is gratefully acknowledged.

References

[1] L.T. Gibson, C.M. Watt, Acetic and formic acids emitted from wood samples and their effect on selected materials in museum environments, Corros. Sci. 52 (2010) 172–178. doi:10.1016/j.corsci.2009.08.054.

[2] L.F.G. Byne, The corrosion of shells in cabinets, J. Conchol. 9 (1899) 172–178.

[3] R. van Tassel, On the crystallography of calclacite, Ca(CH3COO)Cl.5H2O, Acta Crystallogr. 11 (1958) 745–746. doi:10.1107/s0365110x58002000.

[4] A. Boccia Paterakis, M. Steiger, Salt efflorescence on pottery in the Athenian Agora: A closer look, Stud. Conserv. 60 (2015) 172–184. doi:10.1179/2047058413y.0000000113.

[5] J.H.L. Voncken, T.W. Verkroost, M.M. Van Tooren, New powder diffraction data on calclacite (CaClC2H3O2·5H2O), Neues Jahrb. Miner. Monatsh. (2001) 210–220.

[6] G. Giuseppetti, C. Tadini, L. Ungaretti, La struttura cristallina della calclacite/ Crystalline structure of a triclinic phase of the compound corresponding to calclacite, Ca(CH3COO)Cl.5H2O, Period. Di Mineral. 41 (1972) 9–21.

[7] A.F. G. Eggert N. Wahlberg, R. E. Dinnebier, T. Runčevski, R. Kuiter, M. Schüch, S. Kampe, E. Sulzer, A. Wollmann, Efflorescence X? Case Solved: Ca3(CH3COO)3Cl(NO3)2·6H2O! The Research History, Identification, and Crystal Structure of Thecotrichite, in: L.F. H Roemich (Ed.), Recent Adv. Glas. Ceram. Conserv. 2016, International Council of Museums – Committee for Conservation (ICOM-CC), Paris, 2016: pp. 135–144.

[8] N. Wahlberg, T. Runčevski, R.E. Dinnebier, A. Fischer, G. Eggert, B.B. Iversen, Crystal Structure of Thecotrichite, an Efflorescent Salt on Calcareous Objects Stored in Wooden Cabinets, Cryst. Growth Des. 15 (2015) 2795–2800. doi:10.1021/acs.cgd.5b00197.

[9] C. Comel, B.F. Mentzen, Comparative study of the polymorphic species of strontium and calcium

formates. I. Differential thermal analysis (DTA), J. Solid State Chem. 9 (1974) 210–213. doi:10.1016/0022-4596(74)90076-0.

[10] B.F. Mentzen, C. Comel, Comparative study of the polymorphic species of strontium and calcium formates. II. X-Ray diffraction, J. Solid State Chem. 9 (1974) 214–223. doi:10.1016/0022-4596(74)90077-2.

[11] L. Walter-Levy, J. Laniepce, Varieties of anhydrous calcium acetate, Compt. Rend. 250 (1960) 3320–3322.

[12] N.H. Tennent, T. Baird, The deterioration of Mollusca collections: identification of shell efflorescence, Stud. Conserv. 30 (2013) 73–85. doi:10.1179/sic.1985.30.2.73.

[13] E.A. Klop, A. Schouten, P. van der Sluis, A.L. Spek, Structure of calcium acetate monohydrate, Ca(C2H3O2)2.H2O, Acta Crystallogr. Sect. C Cryst. Struct. Commun. 40 (1984) 51–53. doi:10.1107/s0108270184002985.

[14] P. van der Sluis, A. Schouten, A.L. Spek, Structure of a second polymorph of calcium acetate monohydrate, Acta Crystallogr. Sect. C Cryst. Struct. Commun. 43 (1987) 1922–1924. doi:10.1107/s0108270187089601.

[15] R. Helems, L.B. Cole, E.M. Holt, Calcium complexes of mixed ligands: Ca2(acetate)4(HOH)2 and Ca1.5(salicylate)2(acetate)(HOH)2(acetic acid), Inorganica Chim. Acta. 152 (1988) 9–15. doi:10.1016/s0020-1693(00)90724-2.

[16] J. Panzer, Nature of Calcium Acetate, J. Chem. Eng. Data. 7 (1962) 140–142. doi:10.1021/je60012a040.

[17] A. Apelblat, E. Manzurola, Solubilities of magnesium, calcium, barium, cobalt, nickel, copper, and zinc acetates in water fromT= (278.15 to 348.15) K, J. Chem. Thermodyn. 31 (1999) 1347–1357. doi:10.1006/jcht.1999.0548.

[18] L.T. Gibson, B.G. Cooksey, D. Littlejohn, K. Linnow, M. Steiger, N.H. Tennent, The Mode of Formation of Thecotrichite, a Widespread Calcium Acetate Chloride Nitrate Efflorescence, Stud. Conserv. 50 (2005) 284–294. doi:10.1179/sic.2005.50.4.284.

[19] B.G. Cooksey, L.T. Gibson, A.R. Kennedy, D. Littlejohn, L. Stewart, N.H. Tennent, Dicalcium triacetate nitrate dihydrate, Acta Crystallogr. Sect. C Cryst. Struct. Commun. 55 (1999) 324–326. doi:10.1107/s0108270198012864.

[20] R.D. Dooijes M., Preserving the Story of Restored Objects: Combining Technical Data with Historic Sources, in: L.F. H. Roemich (Ed.), Recent Adv. Glas. Ceram. Conserv. 2016., International Council of Museums – Committee for Conservation (ICOM-CC), Paris, 2016: pp. 97–107.

[21] M.R. van B. G. Verhaar N. H. Tennent, Weeping Glass: The Identification of Ionic Species on the Surface of Vessel Glass Using Ion Chromatography, in: L.F. H. Roemich (Ed.), Recent Adv. Glas. Ceram. Conserv. 2016, Committee for Conservation (ICOM-CC), Paris, 2016: pp. 123–125.

[22] TOPAS , (2017).

[23] A.A. Coelho, Indexing of powder diffraction patterns by iterative use of singular value decomposition, J. Appl. Crystallogr. 36 (2003) 86–95. doi:10.1107/s0021889802019878.

[24] A. Le Bail, H. Duroy, J.L. Fourquet, Ab-initio structure determination of LiSbWO6 by X-ray powder diffraction, Mater. Res. Bull. 23 (1988) 447–452. doi:10.1016/0025-5408(88)90019-0.

[25] R.W. Cheary, A.A. Coelho, J.P. Cline, Fundamental Parameters Line Profile Fitting in Laboratory Diffractometers, J Res Natl Inst Stand Technol. 109 (2004) 1–25.

[26] A.A. Coelho, Whole-profile structure solution from powder diffraction data using simulated annealing, J. Appl. Crystallogr. 33 (2000) 899–908. doi:10.1107/s002188980000248x.

[27] V. Favre-Nicolin, R. Černý, FOX: Modular Approach to Crystal Structure Determination from Powder Diffraction, Mater. Sci. Forum. 443–444 (2004) 35–38. doi:10.4028/www.scientific.net/MSF.443-444.35.

[28] H.M. Rietveld, A profile refinement method for nuclear and magnetic structures, J. Appl. Crystallogr. 2 (1969) 65–71. doi:10.1107/s0021889869006558.

[29] WebPDF-4+2016-Database, (2016).

[30] R.S. Krishnan, P.S. Ramanujam, Raman spectrum of calcium formate, J. Raman Spectrosc. 1 (1973) 533–538. doi:10.1002/jrs.1250010603.

[31] P. Baraldi, G. Fabbri, Study of the bands attributable to crystallization water in hydrated metal acetates, Spectrochim. Acta Part A Mol. Spectrosc. 37 (1981) 89–92. doi:10.1016/0584-8539(81)80092-x.

[32] P. Baraldi, Thermal behavior of metal carboxylates: III-metal acetates, Spectrochim. Acta Part A Mol. Spectrosc. 38 (1982) 51–55. doi:10.1016/0584-8539(82)80176-1.

[33] J. Hetmańczyk, Ł. Hetmańczyk, A. Migdał-Mikuli, E. Mikuli, K. Drużbicki, A. Wesełucha-Birczyńska, L.M. Proniewicz, Vibrations and reorientations of H2O molecules and NO3− anions in Ca(H2O)4(NO3)2 studied by incoherent inelastic neutron scattering, Raman light scattering, and infrared absorption spectroscopy, J. Chem. Phys. 131 (2009) 94506. doi:10.1063/1.3202767.

[34] M. Xu, J.P. Larentzos, M. Roshdy, L.J. Criscenti, H.C. Allen, Aqueous divalent metal–nitrate interactions: hydration versus ion pairing, Phys. Chem. Chem. Phys. 10 (2008) 4793. doi:10.1039/b807090n.

[35] E. Spinner, 812. The vibration spectra of some substituted acetate ions, J. Chem. Soc. (1964) 4217–4226. doi:10.1039/jr9640004217.

[36] S. Bette, R.E. Dinnebier, R.K. Kremer, D. Freyer, Ni3Cl2+x(OH)4-x·2H2O: Structural, Thermal, Spectral, and Magnetic Properties in Dependence of the Chloride Content, Eur. J. Inorg. Chem. 2016 (2016) 1875–1885. doi:10.1002/ejic.201600074.

[37] W. Brockner, C. Ehrhardt, M. Gjikaj, Thermal decomposition of nickel nitrate hexahydrate, Ni(NO3)2·6H2O, in comparison to Co(NO3)2·6H2O and Ca(NO3)2·4H2O, Thermochim. Acta. 456 (2007) 64–68. doi:10.1016/j.tca.2007.01.031.

[38] A.W. Musumeci, R.L. Frost, E.R. Waclawik, A spectroscopic study of the mineral paceite (calcium acetate), Spectrochim Acta A Mol Biomol Spectrosc. 67 (2007) 649–661.

[39] Z. Lin, D. Han, S. Li, Study on thermal decomposition of copper(II) acetate monohydrate in air, J. Therm. Anal. Calorim. 107 (2011) 471–475. doi:10.1007/s10973-011-1454-4.

[40] M.O. Bargouth, G. Will, Calcium formate Ca(HCOO)2 (neutron), Cryst. Struct. Commun. 9 (1980) 605–613.

[41] M. Matsui, T. Watanabé, N. Kamijo, R.L. Lapp, R.A. Jacobson, The structures of calcium formate β-Ca(HCOO)2 and δ-Ca(HCOO)2, and the tetragonal mixed crystals Ca(HCOO)2–Sr(HCOO)2, Acta Crystallogr. Sect. B Struct. Crystallogr. Cryst. Chem. 36 (1980) 1081–1086. doi:10.1107/s056774088000533x.

[42] R.E. Dinnebier, T. Runčevski, A. Fischer, G. Eggert, Solid-State Structure of a Degradation Product Frequently Observed on Historic Metal Objects, Inorg. Chem. 54 (2015) 2638–2642. doi:10.1021/ic5027637.

[43] V.O. S. Buys, No Title, in: Conserv. Restor. Ceram., reprint of, Routledge, London, 2011: p. 89.

[44] S. Reguer, F. Mirambet, C. Remazeilles, D. Vantelon, F. Kergourlay, D. Neff, P. Dillmann, Iron corrosion in archaeological context: Structural refinement of the ferrous hydroxychloride β-Fe2(OH)3Cl., Corros. Sci. 100 (2015) 589–598. doi:10.1016/j.corsci.2015.08.035.

[45] M.L. Schlegel, S. Necib, S. Daumas, C. Blanc, E. Foy, N. Trcera, A. Romaine, Microstructural characterization of carbon steel corrosion in clay borehole water under anoxic and transient acidic conditions., Corros. Sci. 109 (2016) 126–144. doi:10.1016/j.corsci.2016.03.022.

[46] M. Bethencourt, T. Fernandez-Montblanc, A. Izquierdo, M.M. Gonzalez-Duarte, C. Munoz-Mas, Study of the influence of physical, chemical and biological conditions that influence the deterioration and protection of Underwater Cultural Heritage., Sci. Total Environ. 613–614 (2018) 98–114. doi:10.1016/j.scitotenv.2017.09.007.